ISSN 0036-0244, Russian Journal of Physical Chemistry A, 2016, Vol. 90, No. 12, pp. 2444–2448. © Pleiades Publishing, Ltd., 2016.
Original Russian Text © A.E. Galashev, L.A. Elshina, R.V. Muradymov, 2016, published in Zhurnal Fizicheskoi Khimii, 2016, Vol. 90, No. 12, pp. 1858–1863.

PHYSICAL CHEMISTRY OF NANOCLUSTERS AND NANOMATERIALS

Molecular Dynamic Study of the Mechanism of Formation of 2D Carbon Nanostructures in a Solid Al–C Nanocomposite Grain

A. E. Galashev*, L. A. Elshina, and R. V. Muradymov

Institute of High-Temperature Electrochemistry, Ural Branch, Russian Academy of Sciences, Yekaterinburg, 620137 Russia
**e-mail: alexander-galashev@yandex.ru*

Received February 15, 2016

Abstract—The behavior of graphene fragments in the structural fcc grains of aluminum was studied by molecular dynamics. In the course of structural relaxation, the graphene sheets united, twisted, and shifted toward the grain boundaries. The structure of the formed nanocomposite grain was studied in detail by statistical geometry. The distributions of Voronoi polyhedra according to the number of faces and of faces according to the number of sides were determined, including those after elimination of small-scale thermal fluctuations from the model. The angular distributions of the nearest geometrical neighbors were calculated, and the self-diffusion coefficients were determined.

Keywords: aluminum, graphene, Voronoi polyhedra, nanocomposite, structural grain

DOI: 10.1134/S0036024416120116

As is known, the solubility of carbon in liquid aluminum is ~0.03 at % [1]. Carbon (graphite) is not wetted by liquid aluminum below 1373 K; therefore, synthesis of an aluminum alloy or composite containing carbon in a concentration higher than equilibrium is an extremely complex problem. One of the authors of the present paper suggested a new method for the formation of carbon inclusions inside metal matrices in concentrations much higher than equilibrium. The one-stage synthesis of atomic carbon is performed directly in a molten metal. In the course of cooling, either cubic diamond and lonsdaleite crystals (2–100 μm) or graphene films (of up to 600 μm^2) form in the bulk of the metal [2, 3].

The mobility of atomic carbon in molten aluminum has the same order of magnitude as in alkali halide melts. As a consequence, the carbon content in aluminum during the interaction of molten aluminum with a carbon-containing halide melt exceeds the known solubility by dozens of times. Various studies showed that graphene films and diamond crystals are present in all metal layers from the surface to the center of the metal sweat ball. The existence of graphene and diamond inclusions in aluminum was confirmed by Raman spectroscopy, and the existence of the local inclusions of cubic diamond and lonsdaleite in aluminum was also confirmed by electron backscattering diffraction. The introduction of 1–2 wt % graphene in aluminum makes it possible to increase the stability, hardness, and elasticity of aluminum–graphene composites by a factor of 1.5–2. Further increase in the graphene content to 5 wt % in the metal matrix leads to an increase in the electrochemical activity, due to which metal–graphene electrodes can be used in electrochemical devices of new generation. Aluminum–graphene composites constitute a new class of construction materials possessing decreased density and increased stability, which will find wide use in aerospace industry [4].

The goal of this study was to investigate the structure formation and peculiarities of the grain of a new aluminum–graphene composite material. This suggests a study of the structural relaxation of the already crystallized Al–C nanocomposite.

COMPUTER MODEL

In the first approximation, the behavior of graphene fragments in the structural grain of aluminum can be considered in a model with free boundary conditions because the atomic diffusion on the boundary of the grain occurs much more readily than in the bulk of it. To take into account the size effect of the system on the formed structure of the nanocomposite, calculations were performed for two systems that differ in the number of Al and C atoms. System I (small) contained 1296 Al and 114 C atoms; system II (large) had 2244 and 318 Al and C atoms, respectively. The concentration of C atoms was 3.77 wt % for system I and 5.93 wt % for system II. Thus, the concentration of C atoms roughly corresponded to the same characteristic of the experimentally obtained nanocomposite samples. The use of higher concentrations for system II makes it possible to verify that the

graphene fragments preserved in the nanocomposite are really stable and to show the absence of three-dimensional carbon formations in the composite if graphite or diamond structures do not form in it. The initial configuration of both systems formed from 13 close-packed (111) aluminum planes. Graphene fragments containing 19 atoms for system I and 53 atoms for system II were embedded in six of these planes in interchanging order. The fragment was formed by five hexagonal honeycomb cells in the former case and 18 in the latter. Each graphene fragment was situated in the middle of the (111) aluminum plane. The distances between the Al and C atoms in this plane were not smaller than the equilibrium distance $r^0_{Al-C} = 2.97$ Å of the corresponding Morse potential [5]. This distance does not exceed the distance between the close-packed planes in aluminum ($r_{Al-Al} = 3.2$ Å). The outer surface of the nanocomposite initially did not contain any C atoms; i.e., it was formed by the perfect aluminum (111) plane. Calculations of 10 million time steps were performed in an NVT ensemble with free boundary conditions using the LAMMPS codes [6]. The time step of integration of the equations of motion was 0.1 fs. The calculations were performed on a URAN computer cluster at the Institute of Mathematics and Mechanics, Ural Branch, Russian Academy of Sciences, with a peak performance of 216 Tflop/s and 1864 CPU.

The model describes the interaction between Al atoms using the Finnis–Sinclair potential [7]. This potential was substantiated from the viewpoint of the electronic solid-state theory. The potential energy of an atomic system U is represented as the sum of the term of atomic pair interactions U_p and the many-particle term U_N identified with the energy of the conductivity electrons:

$$U = U_p + U_N = \frac{1}{2}\sum_{i}^{N}\sum_{j,i\neq j}^{N}\left[(r_{ij}-c)^2\left(c_0 + c_1 r_{ij} + c_2 r_{ij}^2\right)\right] - A\sum_{i}^{N}\sqrt{\sum_{j,i\neq j}(r_{ij}-d)^2},$$

where N is the number of atoms, r_{ij} is the distance between the i and j atoms; c, c_0, c_1, c_2, d, and A are the parameters of the potential [8]; c and d are the cut-off radii for U_p and U_N.

The interaction of C atoms in graphene was described by the second-generation Brenner potential [9]. Correction of the potential allowed not only the reproduction of the equilibrium or quasiequilibrium states of pure carbon, but also an adequate description for hydrocarbonates and reaction modeling. The potential energy limitation at decreased interatomic distance prevented the first-generation Brenner potential [10] from reproducing the atomic collision energy. In the modified variant, the potential explicitly includes the term containing a dihedral angle that describes the important interaction of the π orbitals. This considerably improved the description of the modules that characterize the inflection of graphene, but regretfully did not correct the Young's moduli [11]. The Lennard-Jones interaction between Al and C atoms was introduced with the parameters of the potential taken from [12].

The structure of this film was analyzed in detail by the statistical geometry method. Taking into account the finite size of the systems, the Voronoi polyhedra (VP) were constructed every 10000 time steps for 500 Al atoms of system I and 1000 Al atoms of system II that were closest to the center of mass of the structural grain being modeled. The polyhedra were constructed during the final 2.5 million time steps. The total number of VP for systems I and II was 125000 and 250000, respectively. For C atoms in systems I and II, the VP could not be constructed by the conventional procedure because of the small carbon subsystem and the specifics of the arrangement of C atoms at the nodes of honeycomb cells and the position of the graphene fragments in the MD cells. The typical case of hindrances to the construction of VP here is the absence of geometrical neighbors in one of the semi-spaces allocated for VP construction. Therefore, when constructing the VP for C atoms, we used the method suggested in [13, 14]. The method consists in constructing the VP using the coordinates of the center of mass of the atoms that are candidates for the role of geometrical neighbors, but not from the coordinates of the center of one of the atoms (the central atom).

RESULTS AND DISCUSSION

In scanning electron microscopy (SEM), a thin electron beam (probe) is directed on the sample, generating low-energy secondary electrons, which are collected by a detector. The intensity of the electric signal of the detector mainly depends on the topography of the sample in the region of the interaction. As a result, we obtain a map of the relief of the analyzed zone. Figure 1 shows the presence of graphene films in the surface region of the aluminum–graphene composite revealed by SEM. The graphene sheets lie in different planes and can pile up, twist, and unite with one another.

Figure 2 shows the structure of the composite (system II) obtained by the moment of time 1 ns. The fragments of graphene shown separately on the right side of the MD cell shifted toward the lower part of the calculation cell. The graphene "islands" change in form, but are not destroyed. They approach one another without stacking and form an extended structure resembling a zigzag (staircase). Some of the islands radically changed their initial orientation, and one of them is isolated from the others. Figure 2 shows one C

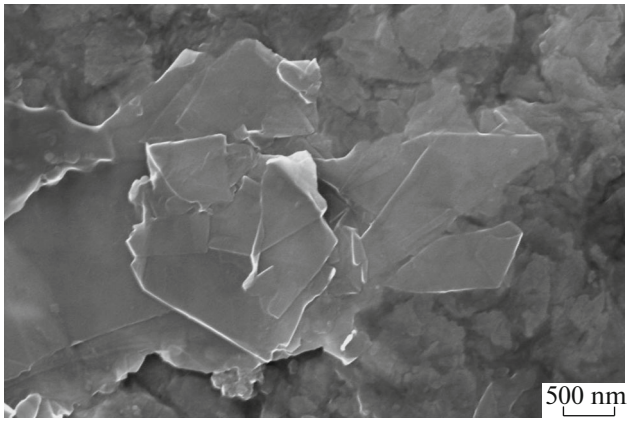

Fig. 1. SEM image of graphene films on the surface of the transverse thin section of the aluminum–graphene composite at large magnification.

atom that departed from graphene. In system I, the graphene fragments were also seen to glide and drift along the aluminum matrix. The moving graphene sheets completely preserved their cellular structure. As a result of these displacements, the graphene sheets united and twisted. The sheets united into hexagonal honeycomb cells at attachment sites. At the moment of connection they could be bent either in the same direction, forming a fragment of the bent surface, or in different directions, forming a wavy ribbon. After 1 ns, the aluminum matrix did not contain two graphene sheets that preserved their initial size (i.e., not linked with another sheet). The sheets had an orientation that was very different from the initial (111) direction. One of them was almost perpendicular to this direction. While moving along the aluminum matrix, the graphene sheets did not lose any one of the C atoms. The structure of the aluminum matrix also underwent considerable changes. However, even in the configuration corresponding to the time 1 ns, rows of atoms and hence crystal ordering can still be traced.

The energies U_{C-C}, U_{Al-Al}, and U_{Al-C} for the large system II are always lower than the corresponding energies for the smaller system I. In the course of calculation, for system I these energies undergo greater changes than for system II. Note that the energy of cross interactions (U_{Al-C}) is negative throughout the calculation and even tends to decrease for system I, reaching its constant value by the end of the calculation. The partial energies finally level off for both systems.

The distribution of VP according to the number of faces n obtained for system II has a maximum at $n = 15$ (Fig. 3). The wide representation of VP in the n spectrum constructed on the basis of the topological characteristic points to considerable structural changes that occurred in the aluminum matrix in the course of the structural relaxation. For close packings, the area of the VP face is proportional to the electron density at the site of the face [15]. Therefore, the n distribution somehow characterizes the stability of the local environment of the atom. Small faces in VP were revealed by excluding the edges with a length $l < \overline{l}$ from the VP, where $\overline{l}$ is the mean edge length. The presence of small geometrical elements (edges and faces) in the VP is explained as manifestation of small-scale thermal fluctuations [16]. The mean number of faces in the VP, $\overline{n} = 13.59$, decreased to 12.40 after the exclusion of small edges from the polyhedra. The distribution of VP according to the number of faces for C atoms obtained in the construction of polyhedra around the center of mass of all geometrical neighbor candidates is shown in the insert of Fig. 3. This distribution includes a still wider spectrum of VP types. The distribution maximum is at $n = 4$; the minimum is at $n = 17$

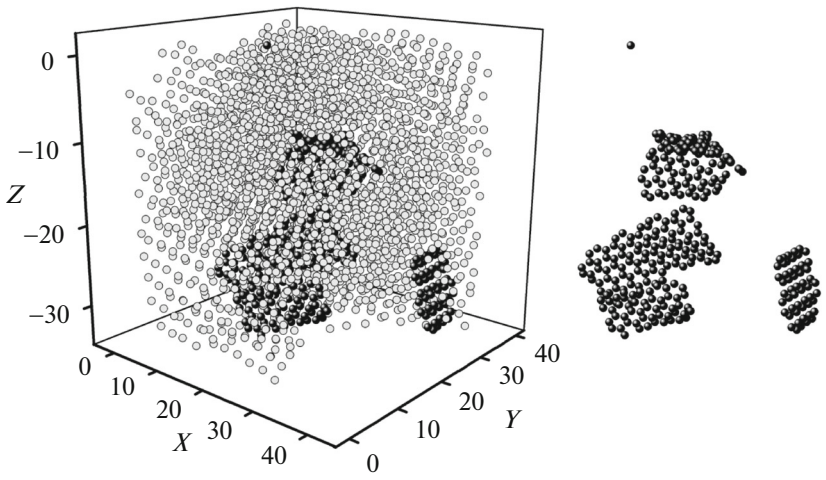

Fig. 2. Configuration of the structural grain of the Al–C nanocomposite that refers to the moment of time 1 ns; the structure of the carbon subsystem is shown on the right; the atomic coordinates are given in angstroms.

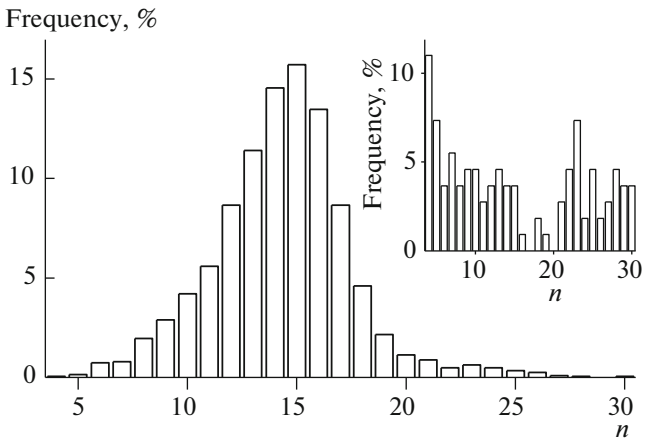

Fig. 3. Distribution of VP according to the number of faces in the aluminum matrix of a system of 2562 atoms. Insert: distribution of VP according to the number of faces for the carbon subsystem based on the construction of polyhedra for the centers of mass of the suggested geometrical neighbors.

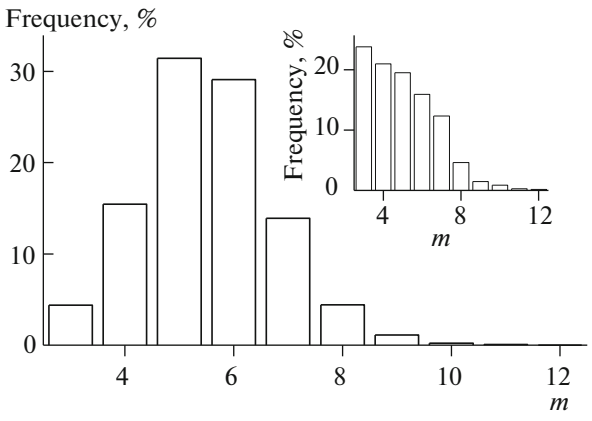

Fig. 4. Distribution of VP faces according to the number of edges in the aluminum matrix of a system of 2562 atoms. Insert: distribution of VP faces according to the number of edges for the carbon subsystem based on the construction of polyhedra for the centers of mass of the suggested geometrical neighbors.

and 20. The U-like type of the n distribution suggests that the arrangement of graphene fragments in the MB cell in the course of structural relaxation is asymmetric.

The distribution of VP faces according to the number m of edges for the Al matrix shown in Fig. 4 for system II is also represented by a wide spectrum. The intensities of the discrete spectrum here determine the relative probability of the statistically average m-fold rotation axis. The maximum of the m distribution lies at $m = 5$, which points to a serious distortion of the crystalline order in the metal matrix. However, the presence of a large fraction of hexagonal faces (92.5% of pentagonal ones) suggests that crystallinity is preserved, at least in the form of close-packed (111) planes in the Al matrix. The average number of edges in the VP faces $\bar{m} = 5.51$ decreased to 5.25 after the exclusion of small geometrical elements from the VP. A similar distribution for the carbon subsystem constructed on the basis of the "specific" VP has a different form (insert, Fig. 4). The trigonal faces are dominant here, and the probability of their appearance decreases as m increases. High m values are generally characteristic for faces with a large area. These faces constitute only a small fraction of the m spectrum. Thus, for the C subsystem, the fraction of faces with $m > 8$ is up to 3%. For truncated polyhedra (with excluded edges) of this subsystem, the tetragonal faces are dominant in the m spectrum (26.1%). There are 25% pentagonal faces and 17.6% trigonal ones.

The angular distribution of the nearest geometrical neighbors for the aluminum matrix of system II has two maxima corresponding to the angles $\theta = 63°$ and 100° and a sloping shoulder in the range $35° \le \theta \le 50°$ (Fig. 5). This θ distribution may be observed for an amorphous solid containing ordered fragments. A pronounced maximum in the vicinity of 60° suggests that the fragments of the close-packed crystal structure are preserved in amorphous aluminum. The average distance to the geometrical neighbor determined by the corresponding VP face in the aluminum matrix was 0.268 nm. The corresponding angular distribution (insert, Fig. 5) constructed with the use of the "specific" polyhedra for the carbon subsystem differs radically from the θ distribution of the aluminum matrix. There is one acute peak at $\theta = 3°$, and the probability of θ angles in the range $6° < \theta \le 180°$ is lower than 0.31; i.e., $\theta \le 6°$ in 69 cases of 100. The high probability of occurrence of C atoms with angles $\theta \le 6°$ is explained by the presence of graphene sheets in the carbon subsystem.

The displacement of graphene fragments in the aluminum matrix of system II is an activation process, as indicated by the behavior of the mean square atomic displacement. The wavy dependence $\left\langle (\Delta r)^2 \right\rangle (t)$ for Al atoms correlates with the behavior of the similar function for C atoms; i.e., the times of appearance of hills and hollows on these curves coincide. The average slope of the dependence $\left\langle (\Delta r)^2 \right\rangle (t)$ determined at the end of the time interval (0.25 ns) for Al atoms is appreciably larger than for C atoms. This points to a larger self-diffusion coefficient for aluminum atoms ($D_{Al} = 8.0 \times 10^{-10}$ m^2/s, $D_C = 2.1 \times 10^{-10}$ m^2/s). The obtained D_{Al} values, however, are much lower than the ab initio calculated self-diffusion coefficient of liquid aluminum (55×10^{-10} m^2/s) [17] at the melting temperature (933.47 K).

The calculated structural characteristics for a smaller system (1296 Al and 114 C atoms) are almost identical to the results obtained for the model of

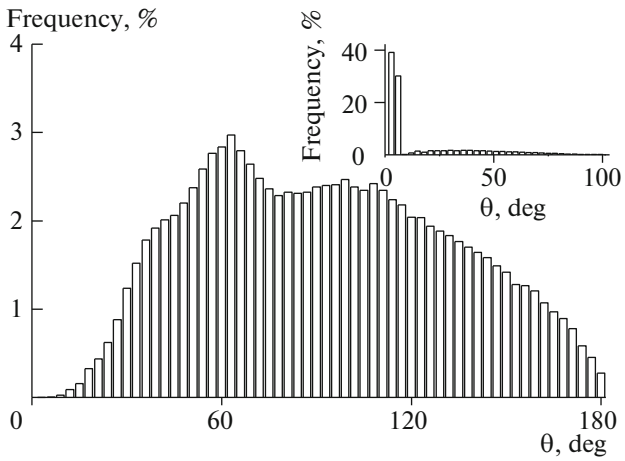

Fig. 5. Angular distribution of the nearest geometrical neighbors in the aluminum matrix of a system of 2562 atoms. Insert: θ distribution for the carbon subsystem based on the construction of polyhedra for the centers of mass of the suggested geometrical neighbors.

2562 atoms. The difference mainly refers to the structural characteristics for the carbon subsystem because the graphene inclusions in system I are smaller. Therefore, the *n* distribution for the carbon component of system I terminates at $n = 19$, but not 30 as for system II. For the *m* distributions, the threshold values of the number of edges in a face are approximately the same for both systems (11 for system I and 12 for system II). For the aluminum matrix in systems I and II, the data are slightly different. For example, for system I, the maximum of VP distribution according to the number of faces lies at $n = 16$ (but not 15), and the shoulder on the left of the first peak in the angular distribution of Al atoms is more pronounced.

Calculations with the EAM potential [18], which is less accurate than the MEAM interatomic interaction potential used by us for aluminum, confirm the final arrangement of graphene fragments near the boundaries of the Al structural grain. When the EAM potential is used, the structural grain is considerably rounded during the observation time 1 ns. That is why the graphene sheets on its surface are severely distorted.

Thus, in the structural grains of the Al–C composite that experienced relaxation (with ~5 wt % graphene), the graphene fragments tend to concentrate along the grain boundaries. This arrangement of graphene inclusions in the metal imparts the material significant extensional compliance and high strength all at once.

REFERENCES

1. B.-H. Liu and Q.-C. Hsu, Mater. Res. Innov. **18** (S3), 65 (2014).
2. L. A. Yolshina, R. V. Muradymov, E. G. Vovkotrub, and S. V. Smirnov, Diamond Rel. Mater. **55**, 1 (2015).
3. L. A. Yolshina, R. V. Muradymov, I. V. Korsun, et al., J. Alloys Compd. **663**, 449 (2016).
4. A. E. Galashev, Tech. Phys. **59**, 467 (2014).
5. T.-H. Fang and J.-H. Wu, Comp. Mater. Sci. **43**, 785 (2008).
6. S. Plimpton, J. Comp. Phys. **117**, 1 (1995).
7. M. W. Finnis and J. E. Sinclair, Philos. Mag. A **50**, 45 (1984).
8. C.-F. Zhu, X.-R. Zhang, Y.-H. Wei, et al., J. Aeronaut. Mater. **23**, 25 (2003).
9. D. W. Brenner, O. A. Shenderova, J. A. Harrison, et al., J. Phys: Condens. Matter **14**, 783 (2002).
10. D. W. Brenner, Phys. Rev. B **42**, 9458 (1990).
11. A. E. Galashev and O. R. Rakhmanova, Phys. Usp. **57**, 970 (2014).
12. S. Xiao and W. Hou, Phys. Rev. B **73**, 115406 (2006).
13. A. N. Novruzov, O. R. Rakhmanova, O. A. Novruzova, and A. E. Galashev, Russ. J. Phys. Chem. B **2**, 115 (2008).
14. A. Y. Galashev, Mol. Simul. **36**, 273 (2010).
15. A. E. Galashev and I. G. Mukhina, Fiz. Met. Metalloved., No. 12, 11 (1992).
16. V. P. Skripov and A. E. Galashev, Russ. Chem. Rev. **52**, 97 (1983).
17. D. J. Gonzalez, L. E. Gonzalez, J. M. Lopez, and M. J. Stott, Phys. Rev. B **65**, 184201 (2002).
18. A. F. Voter and S. P. Chen, Mater. Res. Soc. Symp. Proc. **82**, 175 (1987).

Translated by L. Smolina